

RSC Advances

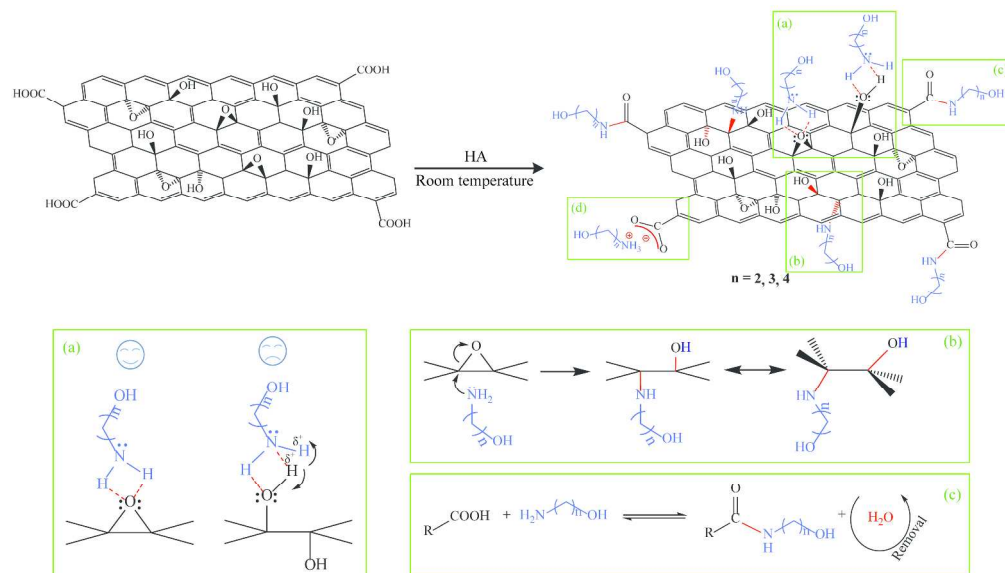


This is an *Accepted Manuscript*, which has been through the Royal Society of Chemistry peer review process and has been accepted for publication.

Accepted Manuscripts are published online shortly after acceptance, before technical editing, formatting and proof reading. Using this free service, authors can make their results available to the community, in citable form, before we publish the edited article. This *Accepted Manuscript* will be replaced by the edited, formatted and paginated article as soon as this is available.

You can find more information about *Accepted Manuscripts* in the [Information for Authors](#).

Please note that technical editing may introduce minor changes to the text and/or graphics, which may alter content. The journal's standard [Terms & Conditions](#) and the [Ethical guidelines](#) still apply. In no event shall the Royal Society of Chemistry be held responsible for any errors or omissions in this *Accepted Manuscript* or any consequences arising from the use of any information it contains.



312x179mm (300 x 300 DPI)



Journal Name

ARTICLE

Understanding room-temperature metastability of graphene oxide utilizing hydramines from a synthetic chemistry view

Yueyue Qian,^a Shupeng Zhang^{*a}, Juanjuan Gao^a and Haiou Song^{*b}

Received 00th January 20xx,
Accepted 00th January 20xx

DOI: 10.1039/x0xx00000x

www.rsc.org/

Owing to polydispersity and polyfunctionality, the chemically controlled heterogeneous synthesis of graphene-based compounds is a great challenge for synthetic chemists. Graphene oxide as significant precursor is playing irreplaceable role for multiple applications. The external temperature stimuli-response process based on the chemistry of graphene oxide is not well understood. An improved fundamental understanding is a crucial prerequisite for their potential application in future. Here, a simple and efficient approach for the synchronized room-temperature surface and edge modification of hydramines (HA) on graphene oxide (GO) is reported. The chemical mechanism investigation of the simultaneous covalent/noncovalent functionalization demonstrates that GO is a metastable material, whose oxygen-containing functional groups could be regarded as active sites and involved in various reactions under such a low temperature. And the size and steric hindrance of substituent of organic molecules play a vital factor to affect the chemical activity. The accurate nanostructures of HA functionalized GO nanomaterials would effectively promote the controlled interfacial engineering of advanced graphene-based nanocomposites.

Introduction

As a rising star in materials science and technology, graphene, a two-dimensional monolayer of carbon atoms arranged in a honey comb lattice, with high physical-chemical properties has been widely applied in various fields.¹⁻³ The control of physical and chemical properties of graphene-based nanomaterials is a challengeable issue for the next generation of nanodevices.⁴ It is very difficult that the inert pristine graphene could be applied directly by simple solution-processed process, though they could be fabricated by expensive chemical vapour deposition^{5,6} or time-consuming micromechanical exfoliation of graphite.⁷ So, the various functionalization strategies have been developed in order to meet practical requirements. Two main approaches have the practical potential. One is to dope heterogeneous atoms onto the basal plane, which is to form covalent bond directly with C atoms of graphene; the other is to establish covalent or noncovalent bond between the functional group native to graphene oxide (GO) and the guest functional group.

Chemical heteroatom-doping in graphene matrix is an effective strategy to tailor the graphene and thus has a large impact on graphene applications, which are gaining more and

more research interests due to their enhanced performance in recent years.^{3,8-11} Especially, the N-doped/modified graphene nanomaterials can improve properties of supercapacitor,^{12,13} electrocatalysts,^{9,10,14} and lithium ion battery³ due to variations of chemical electronic properties of graphene.¹⁵ Several corresponding approaches have been developed including the plasma,¹⁶ arc-discharge of graphite electrodes in a H₂/pyridine or H₂/NH₃ atmosphere,¹¹ chemical vapor deposition¹⁷ and thermal annealing of GO with urea, melamine and cyanamide^{8,15,18,19} etc.^{13,20} These processes accompanying reduction suffer from rigorous conditions and sophisticated equipments, with exposure of poisonous gas and high cost.^{8,12}

As compared to element doping, the functionalization with more complicated organic groups is an easier procedure.²¹ Until now, the most useful method for the large-scale production of functionalized graphene, is still the chemical conversion of graphite to GO, followed by modification of GO. In this process, the direct reduction of GO usually accompanies the agglomeration of reduced graphene without the assistance of other materials, such as polymer etc, which would be obstacle of further application.^{1,2,22,23} So, some typical organic reactions are often utilized to chemically anchor functional groups onto graphene layers to intrigue the enhanced thermal stability, mechanical strength, high processability, etc.^{22,24-27} Many accomplishments have witness the outstanding properties of these approaches including the covalent and noncovalent strategies. But, it is still difficult to achieve complete delamination and functionalization by efficient chemical reactions,^{24,28} though both sides of GO are highly functionalized by oxygen-containing groups as active sites.^{21,29} In addition, owing to polydispersity and polyfunctionality the controlled

^a School of Chemical Engineering, Nanjing University of Science and Technology, Nanjing, Jiangsu, 210094, China. E-mail: shupeng_2006@126.com

^b State Key Laboratory of Pollution Control and Resource Reuse, School of the Environment, Nanjing University, Nanjing, Jiangsu, 210023, China, E-mail: songhaiou2011@126.com

Electronic Supplementary Information (ESI) available: [details of any supplementary information available should be included here]. See DOI: 10.1039/x0xx00000x

wet chemical synthesis of graphene-based compounds is a great challenge for synthetic chemists.²⁴ The two key endeavors are purification and the unambiguous structural confirmation. The introduction of hydrophilic or hydrophobic organic functional groups can successfully prevent agglomeration either by strong electrostatic repulsive forces or owing to their bulky size. It should be noted that the chemical modification of graphene would decrease the electrical conductivity owing to doping insulating molecules and defect concentration on the surface of graphene.³⁰

In the methods mentioned above, GO is usually considered as significant precursor to synthesize various nanomaterials for multiple applications. However, GO in itself, as a material of great interest, its properties should not be neglected. Understanding the chemical transformations occurring in GO in response to external temperature stimuli remains a challenge. An improved fundamental understanding of room-temperature metastability of graphene oxide is a crucial prerequisite for their potential application in future. Herein, a novel route for the simultaneous surface and edge functionalization of GO using HA is adopted to fabricate the supramolecular graphene-based nanohybrids (HA-mGO) through a facile one-step stirring reaction at the room temperature. A comprehensive mechanism picture for this subject in term of how the covalent/noncovalent bonds are formed has been investigated. In this process, HA as an effective nucleophiles can attack the carbon atoms of the ether linkages in GO *via* the typical nucleophilic addition reaction, and the formed sp^3 C-N bonds may suspend the outside of graphene. At the same time, the supramolecular structures can generate between the oxygen functional groups in GO and NH_2 group of HA by hydrogen bonds and electrostatic self-assembly. The introduced organic molecules by the covalent and noncovalent reactions would increase significantly opportunities of "effective collision" for formation of the interfacial interactions. For easy expression, the ethanol amine, amino-1-propanol and 4-amino-1-butanol are represented with AE, AP and AB, respectively. Three compounds are capable of functionalization of GO by a nucleophilic ring opening reaction and supramolecular self-assembly. The accurate nanostructures of HA functionalized GO nanomaterials would effectively promote the controlled interfacial engineering of advanced graphene-based nanocomposites. The investigation of interfacial interaction by combination of HA-mGO and polymer matrix would be evaluated better by enhanced performance of polymer nanocomposites.

Results and discussion

Raman spectroscopy is highly sensitive and nondestructive technique to characterize the structure and quality of carbon materials, particularly to determine the defects, the ordered and disordered structures.³¹ Raman spectra of GO, AB-mGO, AP-mGO and AE-mGO are shown in Fig. 1a. Raman spectra could offer clear evidence of HA functionalization. Generally, Raman spectroscopy of graphene characterized by two prominent peaks: the graphitic (G) peak at about 1575 cm^{-1} , which comes

from the first order scattering of the E_{2g} phonon of the sp^2 carbon atoms and the diamond (D) peak at about 1345 cm^{-1} , which arises from the breathing mode of k-point photons with A_{1g} symmetry.³⁰ The appearance of G (1582 cm^{-1}) and D (1347 cm^{-1}) peaks in higher regions indicates the destruction of the sp^2 character and the formation of defects in the GO nanosheets due to extensive oxidation. And the ratio of D and G band intensity, I_D/I_G , is about 1.0. The I_D/I_G ration of HA-mGO nanomaterials increase from 1.0 for GO to 1.1~1.2, which indicate the formation of more disordered structures. Specially, the highest ratio value for AP-mGO illustrates the best modification degree. And the skeleton structure GO remains in the HA-mGO after functionalization.³²

The FT-IR curve of GO as precursor is shown in Fig. 1b, a strong and broad absorption at 3339 cm^{-1} originated from O-H stretching vibrations can be observed. The characteristic stretching adsorption bands corresponding to the carbonyl groups (C=O) in COOH units situated at edges of GO sheets can be observed at around 1733 cm^{-1} ,^{1,21,25} whereas the bands due to C-O in alcoholic or epoxy groups (COH/COC) appear at 1048 cm^{-1} . In addition, the peak at 1625 cm^{-1} can be attributed to the O-H bending vibration, epoxide groups or skeletal ring vibrations of graphitic domains.^{27,33}

FT-IR spectra are then used to analyze the chemical compositions of HA-mGO nanomaterials. As shown in Fig. 1b and Fig. S1 (see ESI[†]), the new peaks at 2929, 2858, 1605 and 1376 cm^{-1} due to characteristic peaks of hydramines appear in the nanohybrids.³⁴

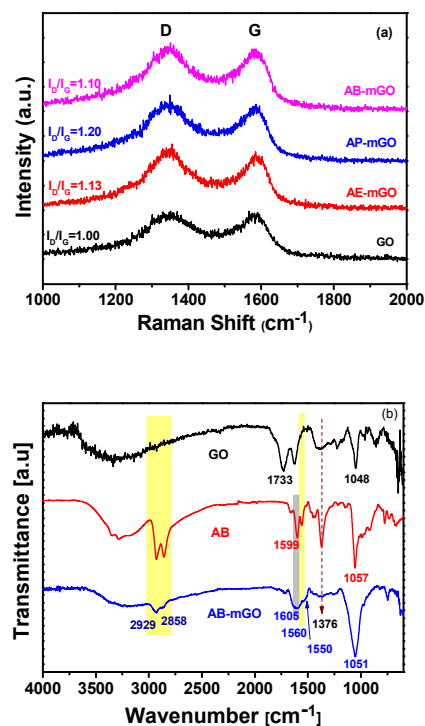


Fig. 1 Raman spectra (a) of GO, AB-mGO, AP-mGO and AE-mGO; FT-IR spectra (b) of GO, AB and AB-mGO as a typical example.

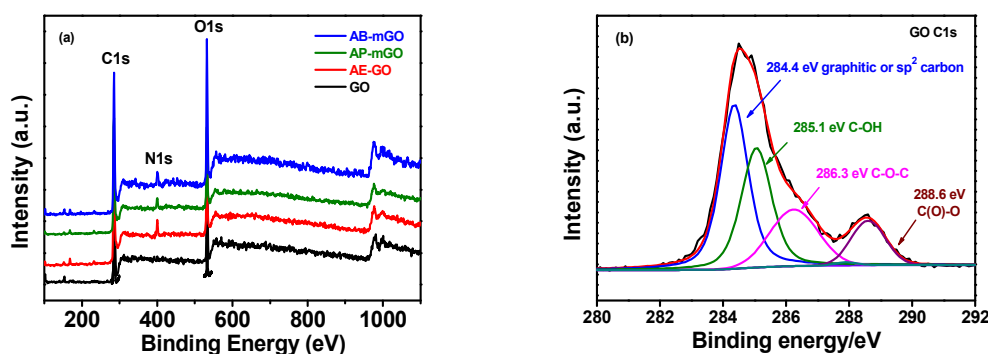
As a typical example, the enhanced intensity of the peak at 1051 cm^{-1} in AB-mGO is observed significantly, which strongly illustrated that the introduction of aliphatic C-N bonds and the peak shift of the alcoholic/epoxy groups from 1048 to 1051 cm^{-1} . The blueshift of 3 cm^{-1} is mainly owing to the generation of more hydrogen bonds between residual oxygen groups of HA-mGO and hydramine. In addition, nitrogen-related peaks appeared at 1560 cm^{-1} in the spectrum of AB-mGO, which can be preliminarily assigned to N-H bending bonds (see ESI Fig. S1†). Furthermore, the content of carbonyl stretching peak of carboxyl groups²⁷ at 1733 cm^{-1} in GO significantly decrease, even disappear in HA-mGO nanomaterials, which may be explained that in the presence of HA, the COOH groups in GO react with the NH_2 in hydramines to generate new chemical bonds, such as carboxylate ($\text{R}^1\text{COONH}_4\text{R}^2$) and amide (R^1CONR^2). A new band at 1550 cm^{-1} assigned to carboxylic acid salt (COO^-) asymmetric stretch mode is observed.²⁷ And, the broader band type from 2400 to 3200 cm^{-1} also could testify the existence of RCOONH_4 structure.

To further evaluate the elemental composition and nitrogen contents of the nonmaterial architectures, X-ray photoelectron spectroscopy (XPS) measurements are performed. As shown in Fig. 2, XPS spectra (Fig. 2a) of GO and HA-mGOs, the corresponding high resolution C1s and N1s spectra of GO (Fig. 2b) and HA-mGOs (Fig. 2c-h) are clearly observed. The XPS spectrum of the GO only shows the existence of the carbon and oxygen atoms. In the case of HA-mGOs, an obvious N signal is evident, and the calculated N/C atomic ratios for AB-mGO, AP-mGO and AE-mGO are 10.66%, 11.26% and 12.31% respectively. This moment, the empirically derived N, C and O atomic sensitivity factors for XPS are 0.25, 0.42 and 0.66.³⁵ And, the N modified level of 7.97% (atom %) achieved for AE-mGO is slightly lower than that (10.1 atom%) of the product fabricated by thermal annealing GO in the presence of melamine at $700\text{ }^\circ\text{C}$.¹⁵

The high-resolution C1s XPS spectrum of GO (Fig. 2b) show four peaks at 284.4, 285.1, 286.3 and 288.6 eV. And they are attributed to graphitic or sp^2 carbon, C-OH, C-O-C and C(O)-O groups, respectively.^{32,36,37} For HA-mGOs, each nanomaterial exhibits one new peak at 287.6 eV corresponding to N- sp^3

carbon bonds (Table 1)³ besides three main peaks above mentioned (Fig. 2d, f and h). The N1s XPS spectrum (Fig. 2c, e and g) was employed to address the bonding chemistry of HA in HA-mGO nanomaterials. Three new peaks for C-N, N-C(O) and NH_3^+-C bonds appears,³² which suggesting that generations (400.8 eV) of covalent amide utilizing COOH and NH_2 of HA molecular containing C-N groups, and electrostatic self-assembly process occurred simultaneously (401.8 eV) (Table 2)

In order to further confirm the origin of C-N signal (399.6 eV), the atom percentages of C-O-C, C-OH and N- sp^3 carbon groups before and after reaction are calculated according to XPS peak fitting data, and listed in Table 1. With the increase of organic molecule chain length from AE to AB, the percentage comparisons of C-O-C groups gradually vary less and less (From 4.77 for AE-mGO to 18.28 for AB-mGO). This observation could be explained with the typical nucleophilic addition mechanism in organic synthesis. Due to the stronger ring strain, epoxides in GO are much more reactive comparing with the simple ethers. As the reaction proceeding, the amino groups (NH_2) of HA could be regarded as nucleophile to attack the electrophilic C of the C-O bonds causing it to break, resulting in ring opening. The opening ring could relieve the ring strain according to the famous nucleophilic addition theory, which belongs to $\text{S}_{\text{N}}2$ type reactions of epoxides. Furthermore, the steric hindrance of each component plays an important role in synthetic reaction based on graphene oxide.²⁸ Especially, for the heterogeneous reaction systems based on GO with rigid structure, AE with shortest chain length can react with active sites very easily. During the process, It should be noted that the hydroxyl groups (OH) in HA would not attack the electrophilic C due to electronic effect, which have been testified in our previous report.²⁷ So, AE with the shortest carbon chain has more opportunities to attack the active sites located at the both sides of GO,^{21,29} which would results in the generation of more OH groups. This moment, the signal at 287.6 eV for AE-mGO should be mainly from the new formation of N- sp^3 carbon groups owing to $\text{S}_{\text{N}}2$ reaction. For the percentages of COOH groups of three products, the obvious decrease can be observed. The chemical bonds owing to the formations of N-C(O) and NH_3^+-C bonds (Estimated by XPS) are formed between GO and HA.



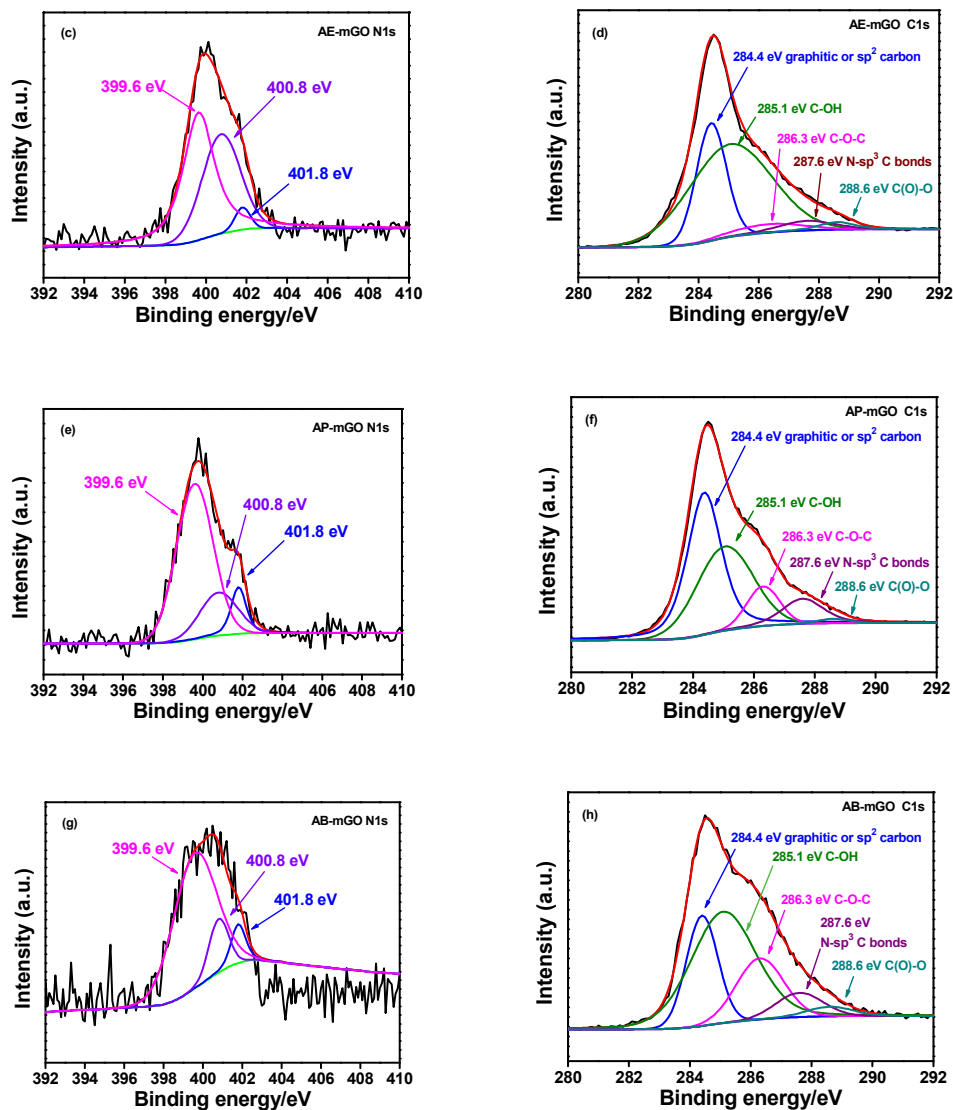


Fig. 2 XPS spectrum (a) of GO, AE-mGO, AP-mGO and AB-mGO, the corresponding high resolution N 1s and C 1s spectra of GO (b) and AE-mGO (c and d), AP-mGO (e and f) and AB-mGO (g and h).

Conversely, AB with longest molecule chain becomes weaker nucleophile due to its steric hindrance, few electrophilic amino groups can attack the electrophilic C of the C-O bonds causing it to break, resulting in ring opening at room temperature. Considering the highest calculated N/C atomic ratios for AB-mGO of 12.31%, we think that the appearance of N- sp^3 carbon bonds is mainly from C-N bonds of AB. That is, the bonds can be mainly introduced by the supramolecular self-assembly based on hydrogen bonds between oxygen-containing functional groups in GO and NH_2 groups of AB.²⁷ Two signals at 400.8 and 401.8 eV in the N1s spectrum suggests the formations of amide and alkylammonium ions (Fig. 2g), as proposed by Matsuo et al.^{38,39}

Similarly, the bonding configurations of nitrogen atoms in HA-mGO are characterized by high-resolution N1s spectra. For example, the N1s spectra of each hybrid material can be fitted into three peaks at 399.6, 400.8 and 401.8 eV (Fig. 2 c, e and g). The peaks with from low to high binding energies, respectively, correspond to C-N, N-C(O) and NH_3^+ -C groups.^{27,38,39} The percentage comparisons of every nitrogen atom groups in HA-mGO are listed in Table 2. Interestingly, the ratios of the N-C(O) and NH_3^+ -C groups are different significantly. Amides (N-C(O)) are commonly formed *via* reactions of a carboxylic acid with an amine. In this chemical reaction, chemical equilibrium is the state in which both reactants and products are present in concentrations which have no further tendency to change with time. Usually, this state results when the forward reaction proceeds at the same rate as the reverse reaction. When

the dynamic equilibrium is disturbed, the changes of concentrations of the reactant and product would appear. For our experiments, H₂O as one of the products can be quickly adsorbed owing to hygroscopicity of HA. Thus, the amounts of generated amide groups would depend on the hygroscopicity of HA. So, for the AE-mGO, the percentage of N-C(O) groups is highest (39.84 %) due to the excellent hygroscopicity of AE. On the contrary, N-C(O) group content of AB-mGO with the poor hygroscopicity is lowest (14.10 %). In addition, it is interesting that maximum amounts of NH₃⁺-C groups based on electrostatic self-assembly can be obtained utilizing AP. The results are possibly due to two main reasons. (1) The steric hindrance would result in more difficult “effective collision” in organic synthesis, especially for the heterogeneous phase reaction systems based on GO. The suitable structural matching between two molecules would optimize the microenvironment and promote the successful possibility of the reaction.²⁸ (2) Besides steric effects, the electronic effects of an arbitrary group in the molecule could also influence the reactivity of organic reactions. HA has the different organic chain length. The CH₂ groups belong to electron-donating substitutes, which could increase the reaction activity of NH₂ groups. But, the electron-donating ability of CH₂ groups is very limited. The ability would rapidly decrease with the increase of distance between the NH₂ and CH₂ groups. At the same time, it should be noticed that OH groups in HA belong to electron withdrawing ones, which could decrease the reaction activity of NH₂ groups. This may be main reason of the lowest percentage comparison of NH₃⁺-C(O) in AE-mGO. So, the obtained results were caused by multiple factors together. Combined with the above Raman, FT-IR and XPS analysis, the HA-mGO could be prepared successfully at the room temperature.

TABLE 1. Percentage comparisons of C-O-C, C-OH and N-sp³ carbon groups with carbon in GO and HA-mGO determined by XPS analysis.

	GO	AE-mGO	AP-mGO	AB-mGO
C-O-C (atom %)	19.16	4.77	9.82	18.28
C-OH (atom %)	30.18	59.81	35.83	49.57
COOH (atom %)	10.71	2.67	0.98	2.78
N-sp³ carbon (atom %)	----	4.77	9.17	7.18

TABLE 2. Percentage comparisons of every nitrogen atom groups in HA-mGO

	AE-mGO	AP-mGO	AB-mGO
C-N (atom %)	56.59	70.01	77.37
N-C(O) (atom %)	39.84	19.73	14.10
NH₃⁺-C(O) (atom %)	3.57	10.26	8.53

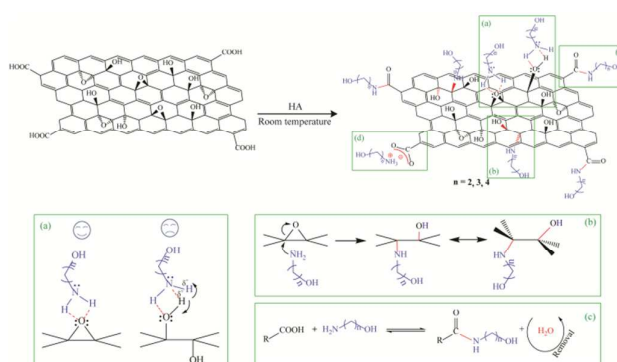


Fig. 3 Schematic for the proposed mechanism of simultaneous room temperature covalent/noncovalent functionalization of GO with HA.

According to the detailed analysis, a proposed mechanism is provided based on previous suggestions reported in the literatures.^{27,38,39} The reaction route and the corresponding active sites are illustrated in Fig. 3, and divided into four regions for the clearer illustration. Graphene is a flat and strain-free system whose plane can be attacked from both sides when dispersed in a solvent.²⁴ Covalent bonds are affected by the electronegativity of the connected atoms. Two atoms with unequal electronegativity will create a polar covalent bond such as with H-N. In HA, the nitrogen atom has the partly negative charges in comparison to hydrogen atom with the partly positive charges. Therefore, the process of transferring the electron from oxygen of GO to hydrogen could take place to create formal charges, the electronic structure may be depicted as in region (a). A noncovalent interaction differs from a covalent bond in that it does not involve the sharing of electrons, but rather involves more dispersed variations of electromagnetic interactions between molecules or within a molecule. And we think that the left coordinate bond structure will be superior to the right one due to additional electrostatic repulsion between two hydrogen atoms with the partly positive charges. In region (b), the addition of HA and the break of the C-O bond would take place simultaneously in the S_N2 reaction (i.e. concerted reaction). S_N2 occurs where the central carbon atom is easily accessible to the nucleophile. And, the mixed usage of an aprotic solvent, DMF and CHCl₃ could not only decrease the polarity of the reaction solution, but also promote the formation of S_N2 reaction transition state. Since this reaction occurs in one step, the reaction speed depends on the sterics strongly. Specially, it is understandable to extremely sterically hinder the reaction based on the GO, which would directly result in the reason of XPS differences. The synthetic reaction of an amide is illustrated in region (c). The amides are formed *via* reactions of a carboxylic acid of GO with an amine of HA. Owing to the hygroscopicity of HA, the H₂O as by-product can be quickly removed from the equilibrium reaction, which would promote the reaction effectively according to the dynamic theory. Thus, the amounts of generated amide groups would depend on the hygroscopicity of HA. Ionic interactions involve the attraction of ions or molecules with full permanent charges of opposite signs. Based on the electrostatic self-

assembly, the interaction between COO^- and NH_3^+ is depicted in region (d). The detailed theoretical analysis fully accord with the results from FT-IR, Raman and XPS characterization.

It should be noticed that the functionalization degree of HA for each type of interactions could not be determined accurately according to the existing results, which would be a great challenge for synthetic chemist. In the future, the development of novel equipments with precision inspection functions would make the impossible possible, just like confirming the organic molecule structure utilizing nuclear magnetic resonance technique. But, the proposed mechanism would provide a better understanding based on graphene chemistry, which would be benefit for the design and fabrication of novel architectures.

In order to investigate the distribution of nitrogen in HA-mGO, the elemental mapping of AE-mGO as a representative example is performed. The nitrogen mapping image (Fig. 4), in accordance with carbon's and oxygen's, actually reflects the morphology of the selective area in Fig. 4. The results confirm that the nitrogen atoms are uniformly distributed in the framework of graphene.

X-ray diffraction peaks determined the changes of interlayer distance of nanosheets shown in Fig. 5. The characteristic XRD diffraction peak of pure GO sheets appeared at $2\theta = 10.2^\circ$ with a d -spacing of 0.88 nm, which is larger than that of pristine graphite (~ 0.34 nm) because of the introduction of oxygen functional groups. After HA functionalization, the diffraction peaks of AB-mGO, AP-mGO and AE-mGO shift to 7.2° , 7.1° and 8.0° , respectively, strongly demonstrating the successful intercalation of HA into the interlayer of graphene nanosheets. Especially, the largest interlayer distance (1.24 nm) of AP-mGO indicates that AP as the most suitable molecule could further increase the exfoliation degree of nanosheets and promote the easier intercalation of polymer for formation of interaction. The result is also supported by SEM images of the AP-mGO nanosheets, as shown in Fig. S2. AP-mGO exhibits the clear layer shape structure. Besides, the broad nature of the diffraction ($2\theta = 21.0^\circ$) indicated poor ordering of the sheets along the stacking direction, implying that the sample is composed mostly of single or few layers of functionalized graphene.⁴⁰ In addition, the thermal stabilities of HA-mGO nanomaterials are superior to the GO (Fig. 6a), which demonstrates that they have been fabricated successfully and can also be regarded as suitable nanofillers to enhance the performance of polymers.

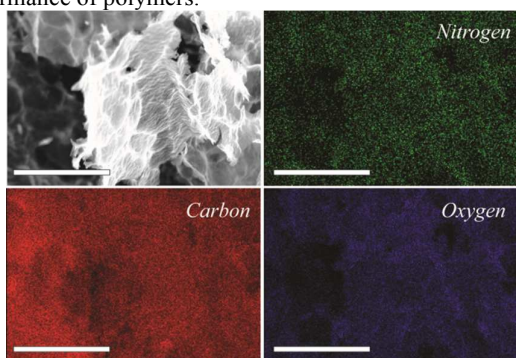


Fig. 4 (b) Carbon, (c) nitrogen and (d) oxygen mapping images of AE-mGO for Fig. 4a. The scale bar is 30 μm .

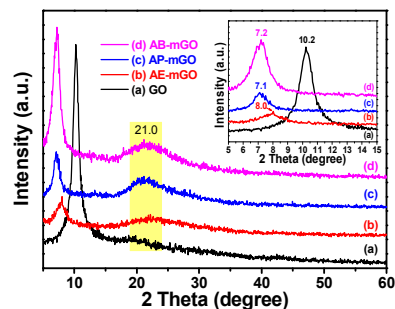


Fig. 5 XRD pattern of GO, AB-mGO, AP-mGO and AE-mGO.

The polymer/graphene nanocomposites have attracted a tremendous amount of attention to obtain high-performance light-weight materials.⁴¹ The functionalized graphene nanomaterials as effective nanofillers have been widely applied in this field.⁴² Graphene-based materials have the potential among all the carbon-based nanofillers due to low production cost, large surface area and low coefficient of thermal expansion.^{42,43} For example, the significant improvement of thermal stability can be observed for the polymer nanocomposites. To achieve maximal performance enhancement, the manufacturing of such nanocomposites requires that the graphene is dispersed homogeneously or best at the molecular level in the matrix and the external load is efficiently transferred *via* a strong interaction at the interface between the graphene and the matrix.⁴⁴ So, the evaluation of the dispersibility of HA-mGO in nine solvents is shown in Fig. S3, which illustrates that HA-mGO can undergo exfoliation completely in water, methanol and dimethylformamide (DMF) etc, it is possible to achieve a truly molecular-level dispersion of HA-mGO in the polymer matrix if the solvent could dissolve the polymer matrix.⁴⁴ On the other hand, the strong interfacial interaction can be formed between these oxygen-containing groups of HA-mGO sheets and polar polymers, which is the internal cause of enhanced properties.⁴⁵ Poly(vinyl alcohol) (PVA) would be chosen as the most suitable matrix due to rich hydroxyl groups.⁴⁶

In order to determine the strong interfacial interactions between oxygen groups on HA-mGO sheets and hydroxyl group on PVA chains, the FT-IR spectra of polymer nanocomposites are investigated. It is well known that the $-\text{OH}$ stretching bands is sensitive to the hydrogen bonding.⁴⁴ The typical bands of PVA and PVA/HA-mGO nanocomposites are shown in Fig. 6b. It can be found that the peaks around 3268 , 2905 and 1087 cm^{-1} , attributed to the characteristic of $-\text{OH}$, $-\text{CH}_2-$ and $\text{C}-\text{O}$ groups, are shifted to the higher wavenumbers for PVA-based nanocomposites with the 1 wt % loading of HA-mGO. The varieties correspond to the formation of the hydrogen bonding between the $-\text{OH}$ in PVA and that in HA-mGO, and generation of hydrophobic interaction between the $-\text{CH}_2-$ groups in PVA and that in HA.²⁷ XRD is another important tool for determining whether graphene-based sheets are indeed present as individual graphene sheets in the nanocomposites.⁴⁴ Fig. 6c and Fig. S4 show the XRD patterns of PVA/HA-mGO nanocomposites

containing 1 wt % nanofillers. As for PVA, the main diffraction peaks at 2θ of 19.6° corresponded to the crystalline region of polymer. After blending the nanofillers, the obviously decreased diffraction peak of PVA ($2\theta=19.6^\circ$) showed a decrease in crystallinity of PVA and indicated that some interactions between PVA chains and the nanofillers may take place.⁴⁷ And two peaks of HA-mGO at $7.1-8.0^\circ$ and 21.0° (Fig. 5) disappeared. These results suggested that the HA-mGO nanosheets are exfoliated absolutely and dispersed at the molecular level into the PVA, which caused the disorder and loss of structure regularity of PVA. Besides, the new main diffraction peak of polymer nanocomposites ($2\theta = 13.7^\circ$) could be observed specially, which is possibly owing to increased interlayer spacing of polymer nanocomposites. To sum up, the intensity of the diffraction peak of PVA nanocomposites slightly raise comparing to pure PVA, which suggests the increased crystallinity of nanocomposites. It is mainly due to the nucleating effect of the fully exfoliated and well-dispersed HA-mGO nanosheets, which could enhance the crystallinity of PVA/HA-mGO.^{44,48,49} But the PVA crystal structure on the surface of nanofillers might not be damaged.^{50,51} Combined with FT-IR and XRD results, it indicates that the strong interfacial interaction must be formed.⁵²

The thermal stability of PVA and PVA/HA-mGO nanocomposites is evaluated by TGA in nitrogen atmosphere, as shown in Fig. 6d. TGA curves of PVA/HA-mGO nanocomposites suggested that the HA-mGO could play a significant role in enhancing the thermal stability of the nanocomposites. The thermal stability of these materials is increased with the lower loading of HA-mGO. Most importantly, almost no weight loss of PVA/AP-mGO nanocomposite occurred at about 50-200 °C, which is attributed to the highest interfacial interaction between PVA and AP-mGO. In comparison to neat PVA, the enhancement of thermal stability can be ascribed to the physical barrier effect of HA-mGO which slowed down the diffusion of pyrolysis products.

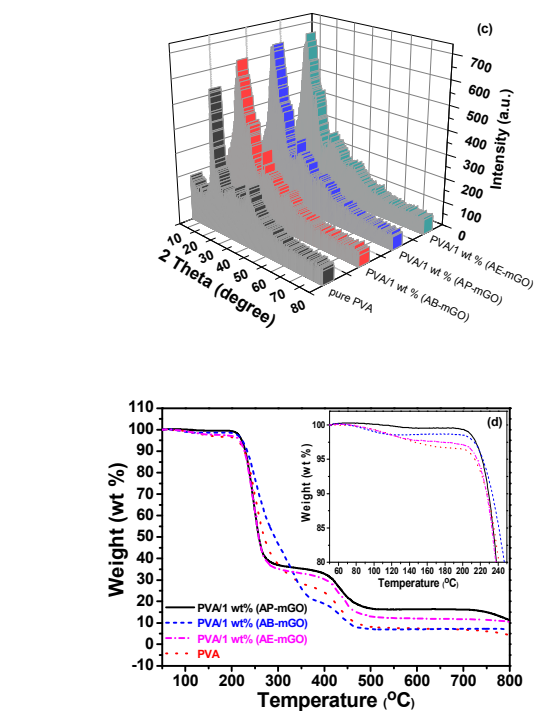
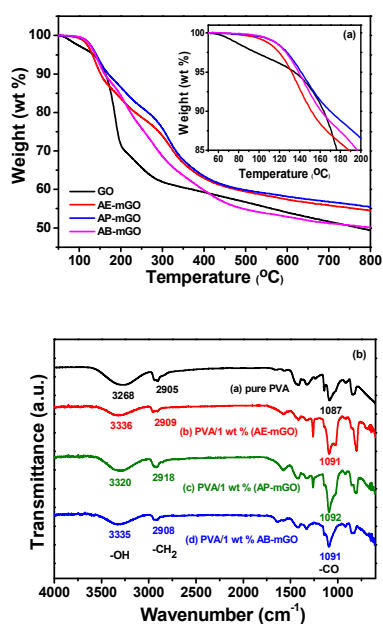


Fig. 6 (a) TGA curves of GO and HA-mGO; (b) FTIR spectra, (c) XRD and (d) thermogravimetric curves of PVA and PVA/HA-mGO nanocomposites.

Conclusions

In summary, a simple, efficient, saving-energy and cost-effective approach for the synchronized surface and edge modification of graphene oxide (GO) utilizing hydramines (HA) has been developed. The simultaneous covalent/noncovalent functionalization process could be completed by continuously stirring the mixture of GO and HA for two days at room temperature. The approach makes the large-scale production of graphene-based materials possible in order to meet the requirement of application. The detailed investigation shows that GO has the property of structural and chemical metastability at room temperature. The proposed reaction mechanism based on the understanding of nucleophilic addition and noncovalent self-assembly would promote the exploration of novel graphene-based nanomaterials for various potential applications. The functionalized nanohybrids (HA-mGO) exhibit the enhanced thermal stability and dispersibility in solvents containing water, strongly supporting that the nanomaterials could be regarded as nanofillers to enhance the performance of polymer nanocomposites.

Acknowledgements

This work was supported by the Natural Science Foundation of China (51402151, 51408297) and the Zijin Intelligent Program,

Nanjing University of Science and Technology. The Natural Science Foundation of Jiangsu province (BK20130575) and Major Science and Technology Program for Water Pollution Control and Treatment, PR China (No. 2014ZX07214-001), the Fundamental Research Funds for the Central Universities (No.20620140479), NUST Graduate Innovation Project (No.149)

Notes and references

- M. H. Rummeli, C. G. Rocha, F. Ortmann, I. Ibrahim, H. Sevincli, F. Börrnert, J. Kunstmann, A. Bachmatiuk, M. Pötsche, M. Shiraishi, M. Meyyappan, B. Büchner, S. Roche and G. Cuniberti, *Adv. Mater.*, 2011, **23**, 4471-4490.
- V. Singh, D. Joung, L. Zhai, S. Das, S. I. Khondaker and S. Seal, *Prog. Mater. Sci.*, 2011, **56**, 1178-1271.
- T. Hu, X. Sun, H. Sun, G. Xin, D. Shao, C. Liu and J. Lian, *Phys. Chem. Chem. Phys.*, 2014, **16**, 1060-1066.
- S. Kim, S. Zhou, Y. Hu, M. Acik, Y. J. Chabal, C. Berger, W. de Heer, A. Bongiorno and E. Riedo, *Nat. Mater.*, 2012, **11**, 544-549.
- P. W. Sutter, J.I. Flege and E. A. Sutter, *Nat. Mater.*, 2008, **7**, 406-411.
- P. S. Toth, Q. M. Ramasse, M. Velicky and R. A. W. Dryfe, *Chem. Sci.* 2015, **6**, 1316-1323.
- K. S. Novoselov, A. K. Geim, S. V. Morozov, D. Jiang, Y. Zhang, S. V. Dubonos, I. V. Grigorieva and A. A. Firsov, *Science*, 2004, **306**, 666-669.
- Y. Zhao, C. Hu, L. Song, L. Wang, G. Shi, L. Dai and L. Qu, *Energy Environ. Sci.*, 2014, **7**, 1913-1918.
- L. Qu, Y. Liu, J.B. Baek and L. Dai, *ACS Nano*, 2010, **4**, 1321-1326.
- K. Gong, F. Du, Z. Xia, M. Durstock and L. Dai, *Science*, 2009, **323**, 760-764.
- L. S. Panchakarla, K. S. Subrahmanyam, S. K. Saha, A. Govindaraj, H. R. Krishnamurthy, U. V. Waghmare and C. N. R. Rao, *Adv. Mater.*, 2009, **21**, 4726-4730.
- Y. Lu, F. Zhang, T. Zhang, K. Leng, L. Zhang, X. Yang, Y. Ma, Y. Huang, M. Zhang and Y. Chen, *Carbon*, 2013, **63**, 508-516.
- F. M. Hassan, V. Chabot, J. Li, B. K. Kim, L. Ricardez-Sandoval and A. Yu, *J. Mater. Chem. A*, 2013, **1**, 2904-2912.
- Z.S. Wu, S. Yang, Y. Sun, K. Parvez, X. Feng and K. Müllen, *J. Am. Chem. Soc.*, 2012, **134**, 9082-9085.
- Z.H. Sheng, L. Shao, J.J. Chen, W.J. Bao, F.B. Wang and X.-H. Xia, *ACS Nano*, 2011, **5**, 4350-4358.
- Y. Wang, Y. Shao, D. W. Matson, J. Li and Y. Lin, *ACS Nano*, 2010, **4**, 1790-1798.
- Y. Xue, B. Wu, L. Jiang, Y. Guo, L. Huang, J. Chen, J. Tan, D. Geng, B. Luo, W. Hu, G. Yu and Y. Liu, *J. Am. Chem. Soc.*, 2012, **134**, 11060-11063.
- Z. Lin, G. Waller, Y. Liu, M. Liu and C.-P. Wong, *Adv. Energy Mater.*, 2012, **2**, 884-888.
- Z. Wen, X. Wang, S. Mao, Z. Bo, H. Kim, S. Cui, G. Lu, X. Feng and J. Chen, *Adv. Mater.*, 2012, **24**, 5610-5616.
- Z.S. Wu, W. Ren, L. Xu, F. Li and H.M. Cheng, *ACS Nano*, 2011, **5**, 5463-5471.
- D. R. Dreyer, S. Park, C. W. Bielawski and R. S. Ruoff, *Chem. Soc. Rev.*, 2010, **39**, 228-240.
- Y. Zhu, S. Murali, W. Cai, X. Li, J. W. Suk, J. R. Potts and R. S. Ruoff, *Adv. Mater.*, 2010, **22**, 3906-3924.
- Y.T. Liu, X.M. Xie, and X.Y. Ye, *Carbon*, 2011, **49**, 3529-3537.
- S. Eigler and A. Hirsch, *Angew. Chem. Int. Ed.*, 2014, **53**, 7720-7738.
- S.P. Zhang, P. Xiong, X.J. Yang and X. Wang, *Nanoscale*, 2011, **3**, 2169-2174.
- L. Yan, Y. B. Zheng, F. Zhao, S. Li, X. Gao, B. Xu, P. S. Weiss and Y. Zhao, *Chem. Soc. Rev.*, 2012, **41**, 97-114.
- S.P. Zhang and H.O. Song, *New J. Chem.*, 2012, **36**, 1733-1738.
- J.J. Gao, S.P. Zhang, X. Zhang, C.P. Yu, H.L. Ye, Y.Y. Qian and H.O. Song, *RSC Adv.*, 2014, **5**, 3954-3958.
- A. Lerf, H. He, M. Forster and J. Klinowski, *J. Phys. Chem. B*, 1998, **102**, 4477-4482.
- N. H. Kim, T. Kuila and J. H. Lee, *J. Mater. Chem. A*, 2013, **1**, 1349-1358.
- A. Das, S. Pisana, B. Chakraborty, S. Piscanec, S. K. Saha, U. V. Waghmare, K. S. Novoselov, H. R. Krishnamurthy, A. K. Geim, A. C. Ferrari and A. K. Sood, *Nat. Nanotechnol.*, 2008, **3**, 210-215.
- O. C. Compton, D. A. Dikin, K. W. Putz, L. C. Brinson and S. T. Nguyen, *Adv. Mater.*, 2010, **22**, 892-896.
- C. Zhang, R. Hao, H. Liao and Y. Hou, *Nano Energy*, 2013, **2**, 88-97.
- Y. Cao, J. Feng and P. Wu, *Carbon*, 2010, **48**, 1683-1685.
- C. D. Wagner, L. E. Davis, M. V. Zeller, J. A. Taylor, R. H. Raymond and L. H. Gale, *Surf. Interface Anal.*, 1981, **3**, 211-225.
- S. Stankovich, D. A. Dikin, R. D. Piner, K. A. Kohlhaas, A. Kleinhammes, Y. Jia, Y. Wu, S. T. Nguyen and R. S. Ruoff, *Carbon*, 2007, **45**, 1558-1565.
- X. Dong, C.Y. Su, W. Zhang, J. Zhao, Q. Ling, W. Huang, P. Chen and L.J. Li, *Phys. Chem. Chem. Phys.*, 2010, **12**, 2164-2169.
- Y. Matsuo, T. Miyabe, T. Fukutsuka and Y. Sugie, *Carbon*, 2007, **45**, 1005-1012.
- Z. Liu, X. Duan, G. Qian, X. Zhou and W. Yuan, *Nanotechnology*, 2013, **24**, 045609.
- A. V. Murugan, T. Muraliganth and A. Manthiram, *Chem. Mater.*, 2010, **22**, 2692-2692.
- R. Verdejo, M. M. Bernal, L. J. Romasanta and M. A. Lopez-Manchado, *J. Mater. Chem.*, 2011, **21**, 3301-3310.
- T. Kuilla, S. Bhadra, D. Yao, N. H. Kim, S. Bose and J. H. Lee, *Prog. Polym. Sci.*, 2010, **35**, 1350-1375.
- Y. Si and E. T. Samulski, *Nano Lett*, 2008, **8**, 1679-1682.
- J. J. Li, L. S. Shao, L. H. Yuan and Y. H. Wang, *Mater. Design*, 2014, **54**, 520-525.
- J. J. Liang, Y. Huang, L. Zhang, Y. Wang, Y. F. Ma, T. Y. Guo and Y. S. Chen, *Adv. Funct. Mater.*, 2009, **19**, 2297-2302.
- Y. X. Xu, W. J. Hong, H. Bai, C. Li and G. Q. Shi, *Carbon*, 2009, **47**, 3538-3543.
- X. Yang, L. Li, S. Shang and X.M. Tao, *Polymer*, 2010, **51**, 3431-3435.
- C. Bao, Y. Guo, L. Song and Y. Hu, *J. Mater. Chem.*, 2011, **21**, 13942-13950.
- X. Zhao, Q. Zhang, D. Chen and P. Lu, *Macromolecules*, 2010, **43**, 2357-2363.
- N. Chen, Y.T. Liu, X.M. Xie, X.Y. Ye, X. Feng, Y.F. Chen and Y.H. Wang, *Carbon*, 2012, **50**, 4760-4764.
- J.Z. Xu, T. Chen, C.L. Yang, Z.M. Li, Y.M. Mao, B.Q. Zeng and B.S. Hsiao, *Macromolecules*, 2010, **43**, 5000-5008.
- Y.T. Liu, J.M. Yang, X.M. Xie, and X.Y. Ye, *Mater. Chem. Phys.*, 2011, **130**, 794-799.